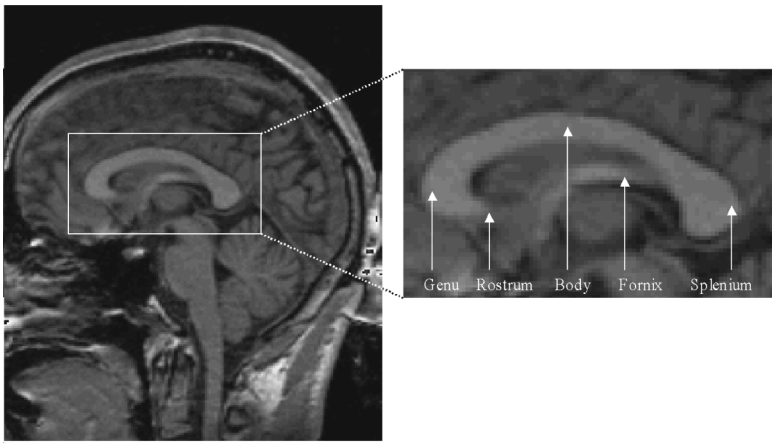

Figure 1. Corpus callosum anatomy overlain on a midsagittal MRI brain slice.

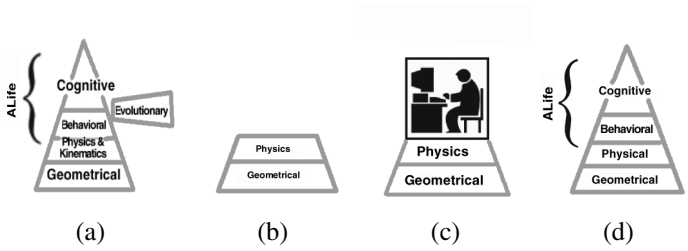

Figure 2. AL, Deformable Models, and Deformable Organisms. (a) AL modeling pyramid. Adapted with permission from [39]. Copyright ©1999, ACM. (b) Automatic deformable models (incorporating geometry and physics layers only). (c) Deformable models guided by an expert human operator. (d) Intelligent deformable models (deformable organisms) provide a model of the cognitive abilities of human operators (by including higher cognitive layers).

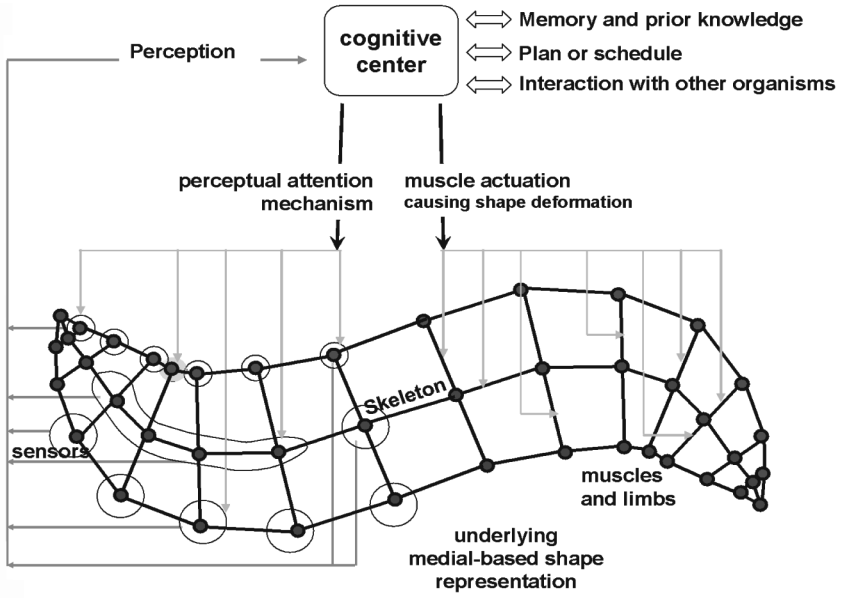

Figure 3. A Deformable Organism. The brain issues "muscle" actuation and perceptual attention commands. The organism deforms and senses image features, whose characteristics are conveyed to the brain. The brain makes decisions based on sensory input, memorized information and prior knowledge, and a pre-stored plan, which may involve interaction with other organisms. Reprinted with permission from [85]. Copyright ©2002, Elsevier.

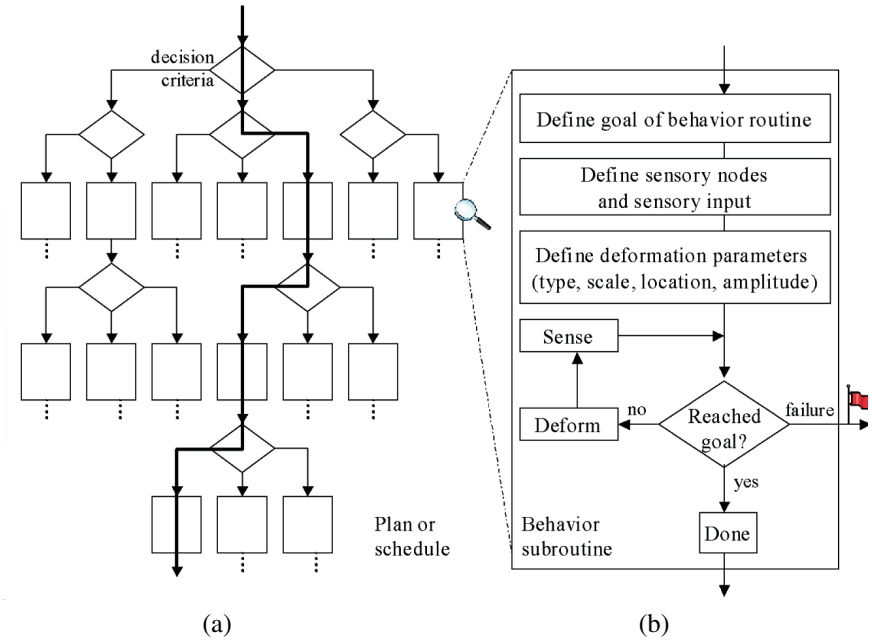

Figure 4. (a) Procedural representation of a fragment of a deformable organism's plan or schedule. The organism goes through several behavior subroutines (bold path in (a)). (b) Generic example of a behavior routine. Reprinted with permission from [85]. Copyright ©2002, Elsevier.

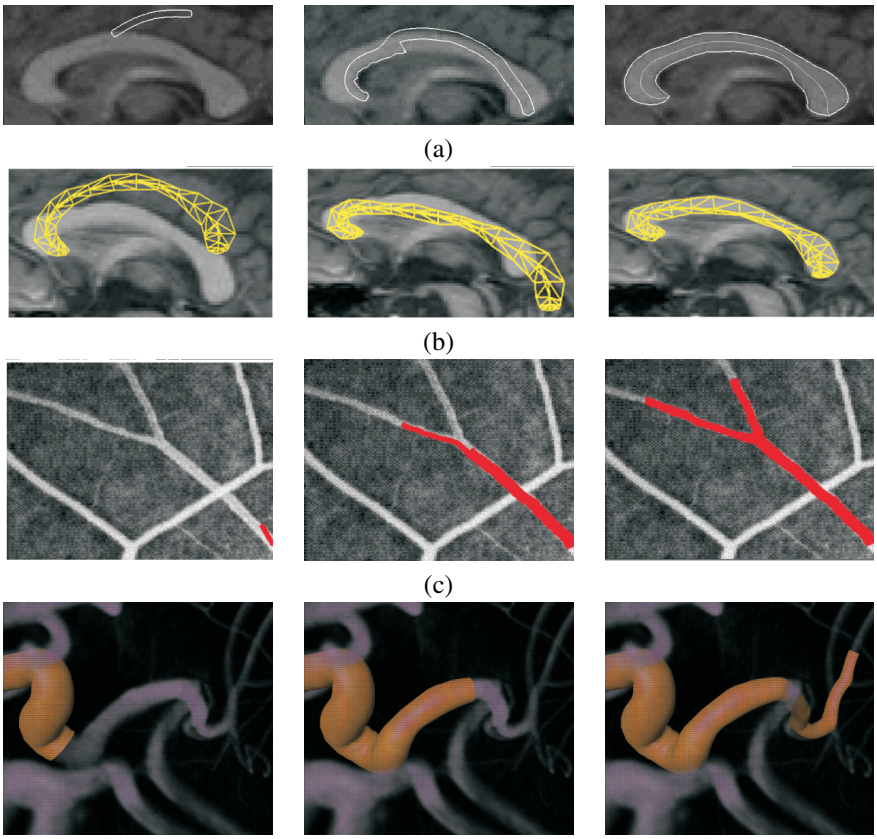

Figure 5. Example deformable organisms for medical image analysis. (a) Geometrically based and (b) physically based deformable CC organisms. (c) 2D and (d) 3D vessel crawler. Progress of segmentation is shown from left to right.

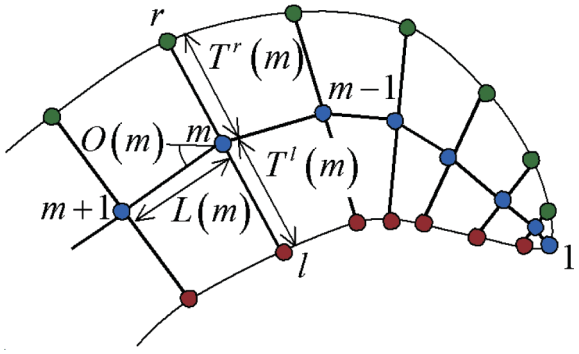

Figure 6. Diagram of shape representation. Reprinted with permission from [85]. Copyright ©2002, Elsevier.

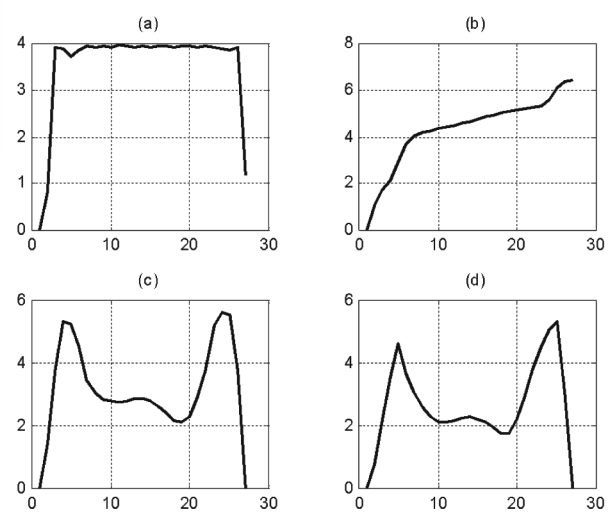

Figure 7. Example medial shape profiles: (a) length profile $L(m)$, (b) orientation profile $O(m)$, (c) left thickness profile $T^l(m)$, and (d) right thickness profile $T^r(m)$. Reprinted with permission from [85]. Copyright ©2002, Elsevier.

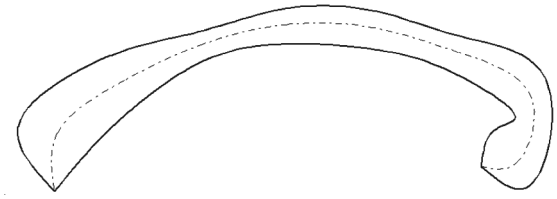

Figure 8. Object reconstruction resulting from the shape profiles in Figure 7

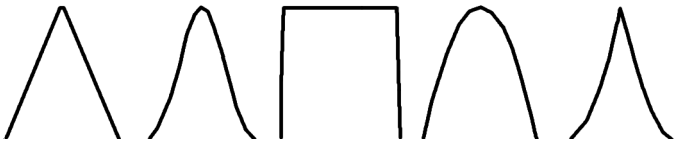

Figure 9. Examples of operator types: (left to right) triangular, Gaussian, flat, bell, and cusp [75]. Reprinted with permission from [63]. Copyright ©2004, World Scientific.

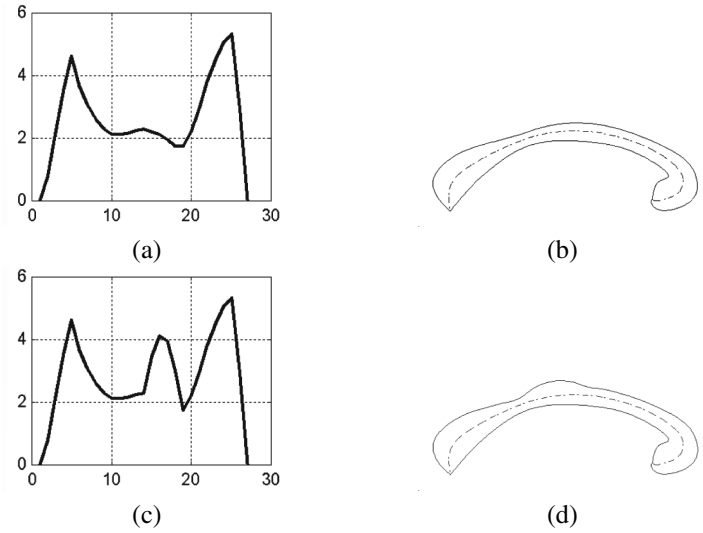

Figure 10. Introducing a bulge on the right boundary by applying a deformation operator on the right thickness profile: (a) $T^r\,(m)$ before and (c) after applying the operator. (b) Reconstructed shape before and (d) after the operator. Reprinted with permission from [85]. Copyright ©2002, Elsevier.

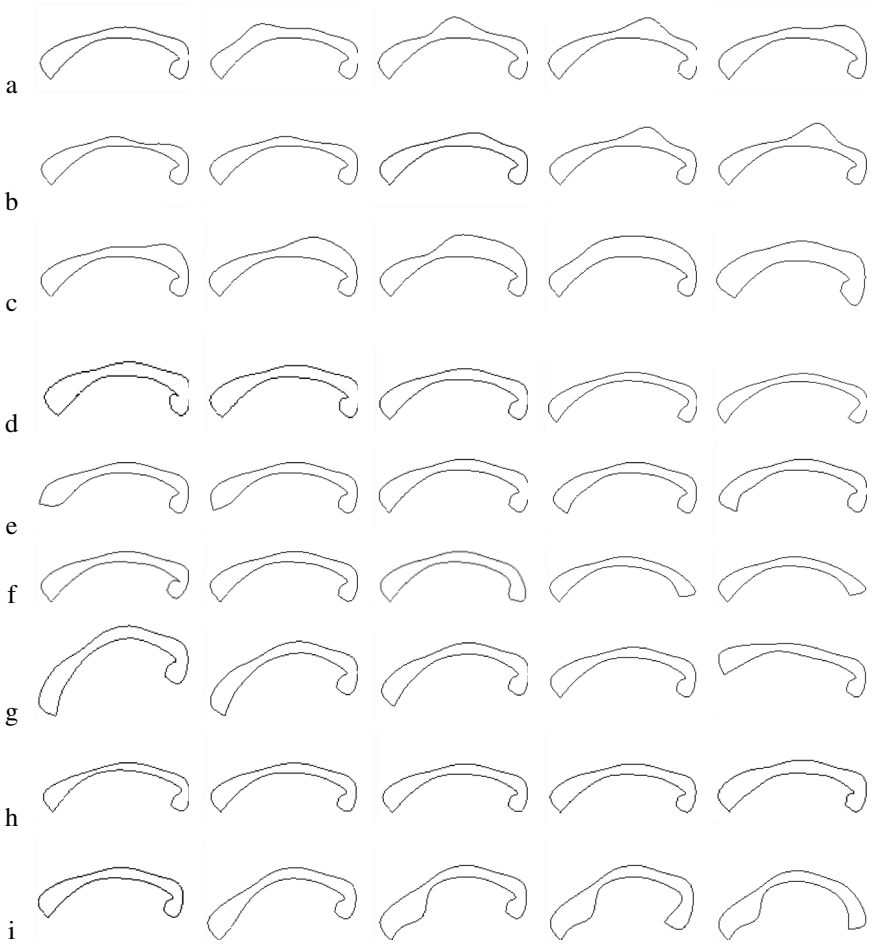

Figure 11. Examples of Controlled Deformations. (a)–(c) Operator-based bulge deformation at varying locations, amplitudes, and scales. (d) Operator-based stretching with varying amplitudes over entire CC. (e)–(g) Statistics-based bending of the left end, the right end, and the left half of the CC. (h) Statistics-based bulge of the left and right thickness over the entire CC. (i) From left to right: (1) mean shape, (2) statistics-based bending of the left half, followed by (3) locally increasing the left thickness using an operator, followed by (4) applying an operator-based stretch and (5) an operator-based bend to the right side of the corpus callosum. Reprinted with permission from [63]. Copyright ©2004, World Scientific.

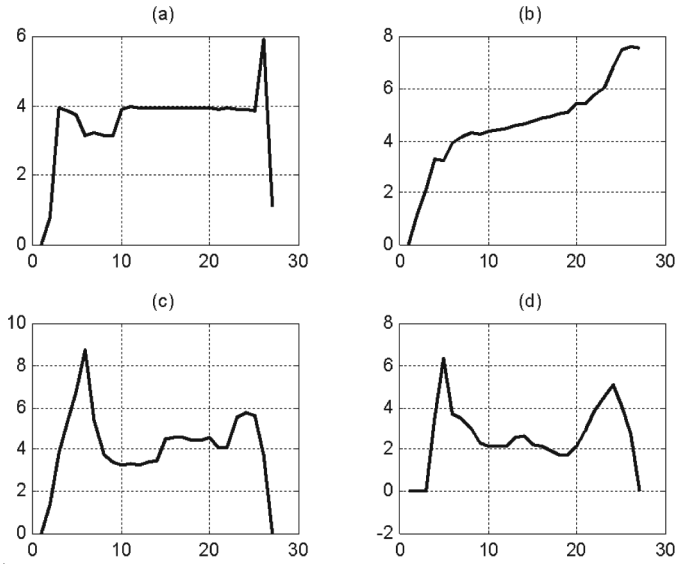

Figure 12. Resulting medial shape profiles after applying the fitting schedule: (a) length profile $L\,(m)$, (b) orientation profile $O\,(m)$, (c) left thickness profile $T^l\,(m)$, and (d) right thickness profile $T^r\,(m)$. Reprinted with permission from [63]. Copyright ©2004, World Scientific.

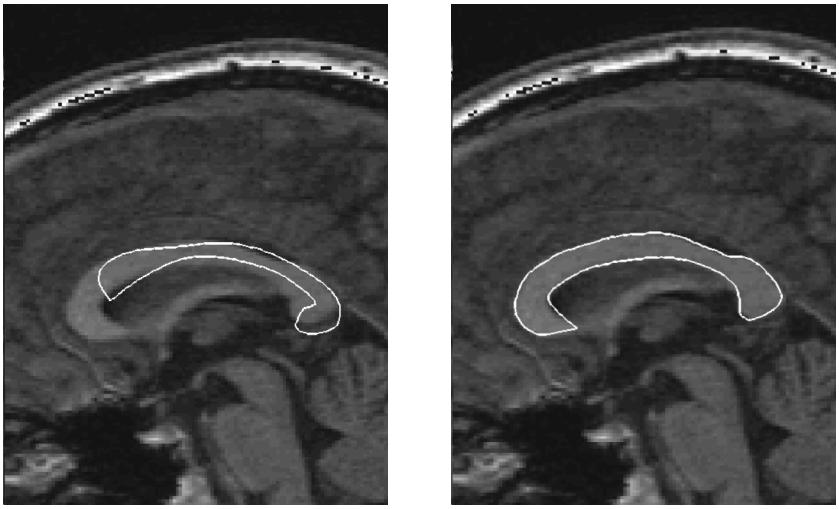

Figure 13. Close-up of the initial and final stages of the handcrafted fitting schedule. Reprinted with permission from [63]. Copyright ©2004, World Scientific.

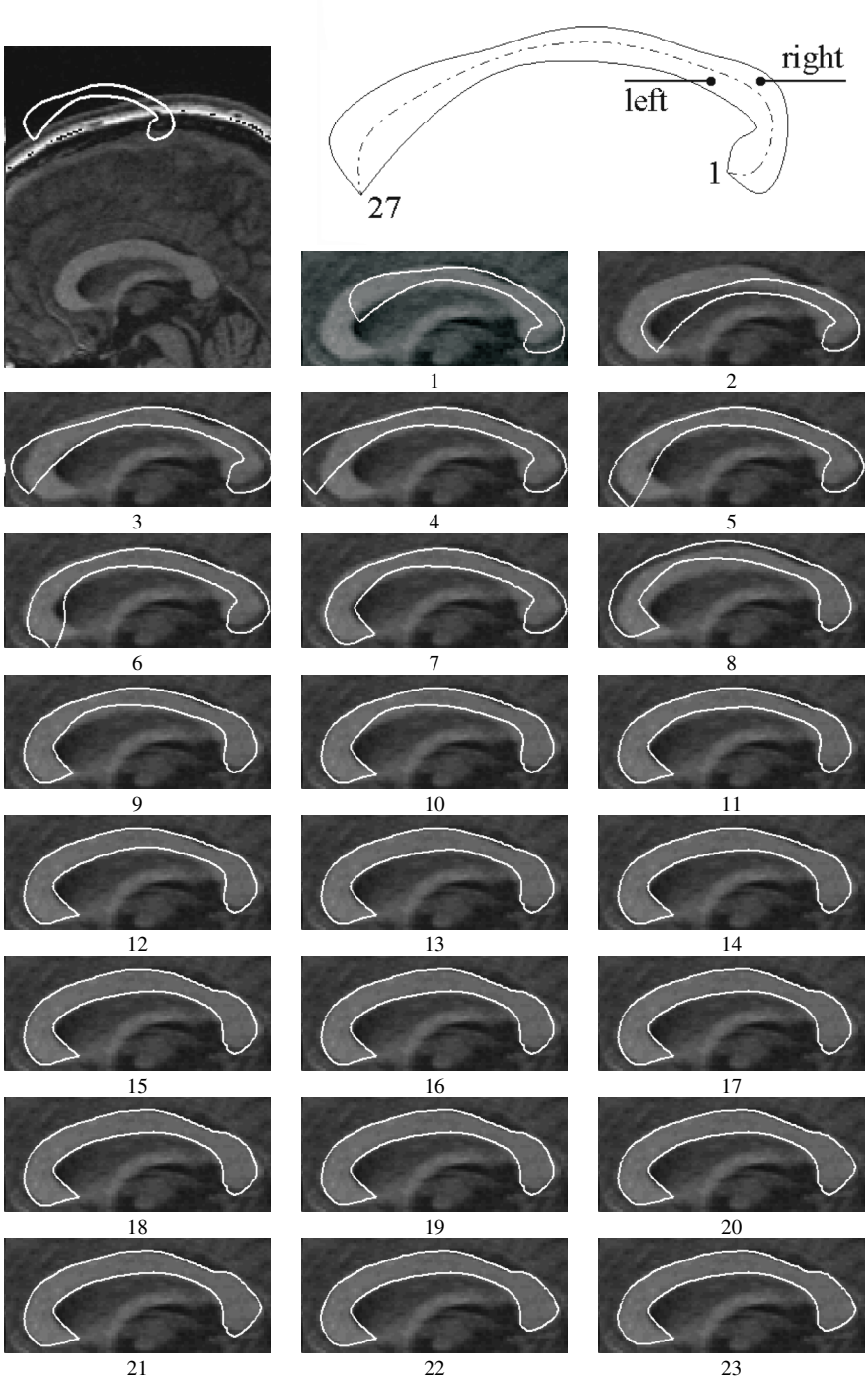

Figure 14. Progress of the handcrafted fitting schedule (fitting steps listed in Table 1). Reprinted with permission from [63]. Copyright ©2004, World Scientific.

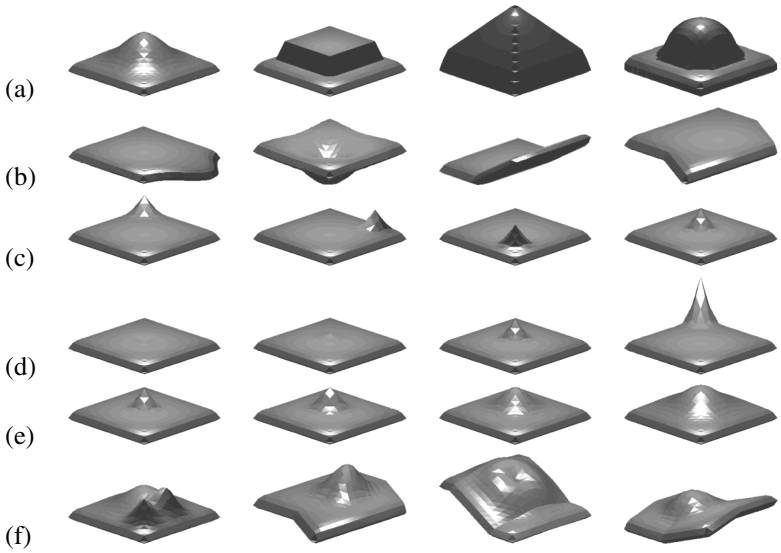

Figure 15. Deformations on a synthetic (slab) object. (a) Different operator types (left to right): Gaussian, rectangular, pyramidal, spherical. (b) Different deformation types: stretching, longitudinal bend, latitudinal bend. Different (c) locations, (d) amplitudes, and (e) extent of a bulge operator. (f) Combining stretching, longitudinal and latitudinal bend, and bulging deformations.

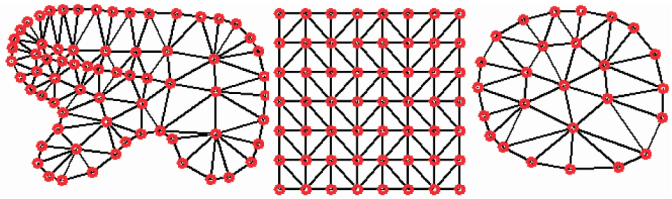

Figure 16. Examples of different synthetic spring-mass structures. Reprinted with permission from [80].

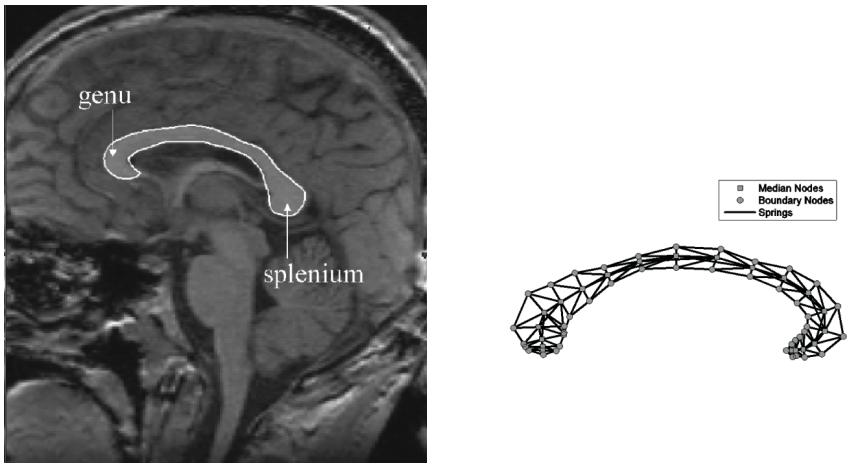

Figure 17. (a) Midsagittal MR brain image with the corpus callosum (CC) outlined in white. (b) CC mesh model showing medial and boundary masses. Reprinted with permission from [80]. Copyright ©2005, SPIE.

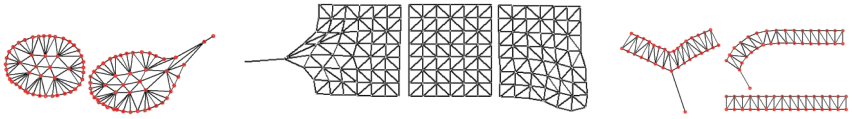

Figure 18. Examples of deformations via user interaction ("mouse" forces). Reprinted with permission from [62]. Copyright ©2003, SPIE.

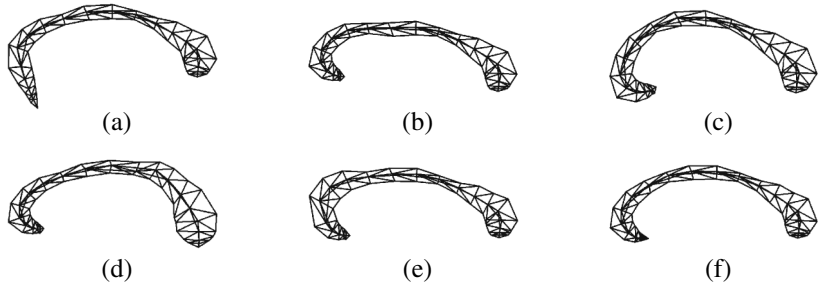

Figure 19. Examples of physics-based deformations of the CC organism using (a) user applied and (b) rotational external forces. Operator based (c) bending, (d) bulging, and (e) stretching deformations. (f) Statistics-based spring actuation. Reprinted with permission from [62]. Copyright ©2003, SPIE.

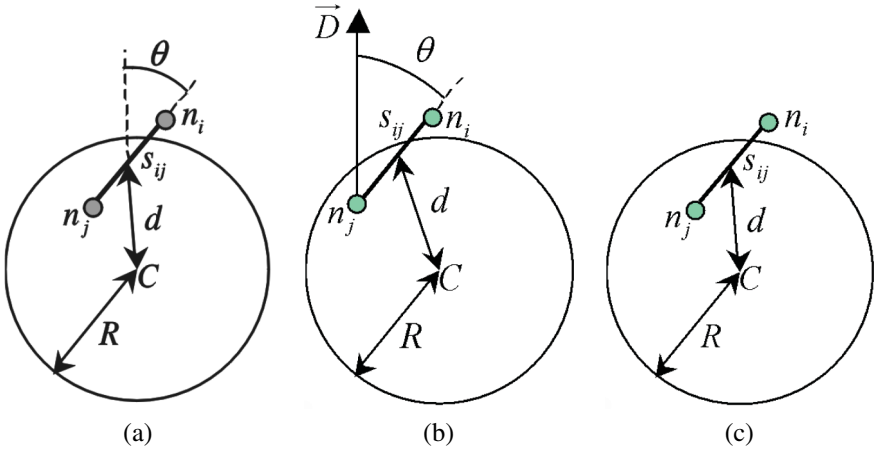

Figure 20. Definition of variables for (a) radial bulge, (b) directional bulge, and (c) localized scaling.

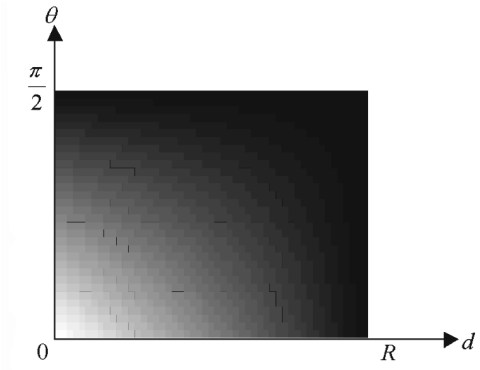

Figure 21. The coefficient (white = K, black = 1) by which r_{ij}^{old} is multiplied as a function of θ and d. Reprinted with permission from [62]. Copyright ©2003, SPIE.

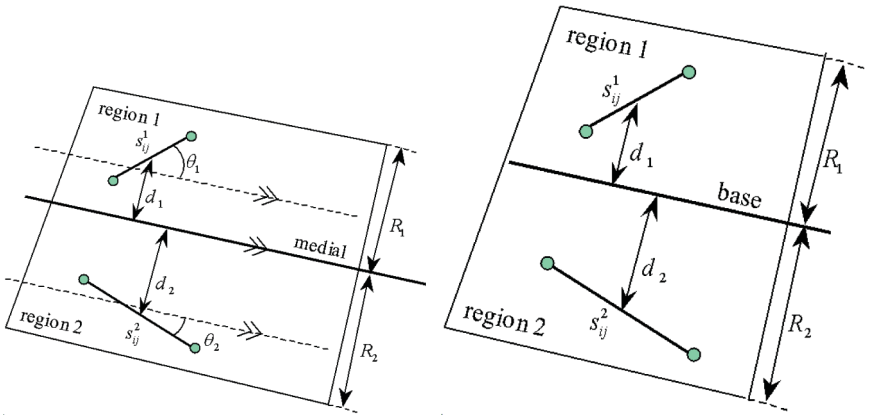

Figure 22. Definition of variables for deformation operators: bending (left), and tapering (middle). Reprinted with permission from [62]. Copyright ©2003, SPIE.

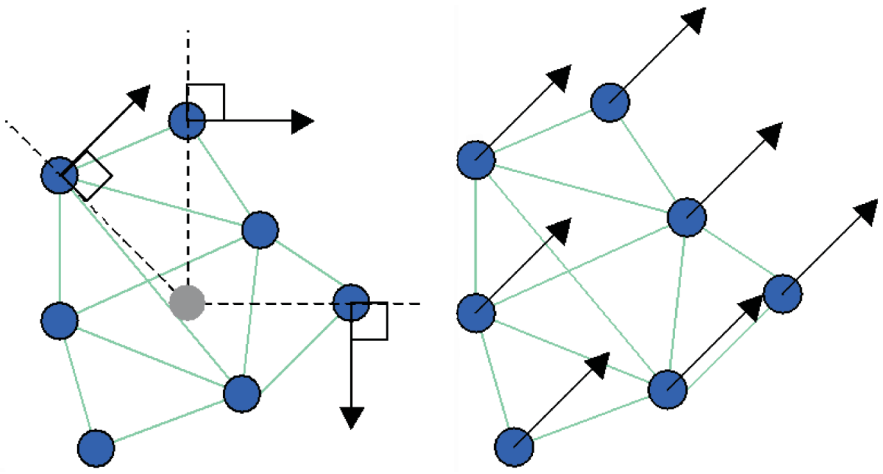

(a) (b)

Figure 23. External forces for performing a (a) rotation (light gray circle marks center of mass) and a (b) translation. Reprinted with permission from [62]. Copyright ©2003, SPIE.

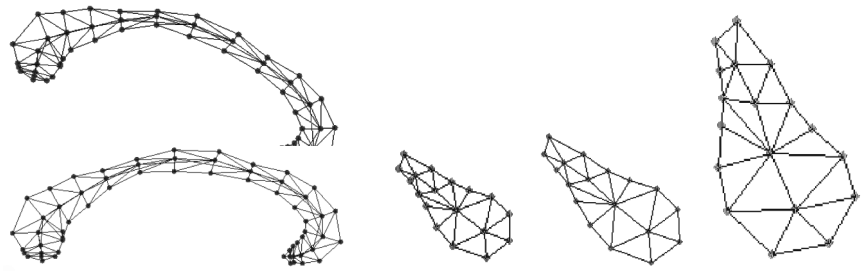

Figure 24. Similarity transformation via external forces. (a) Rotating a model of the CC. (b) Scaling and rotating a synthetic model. Reprinted with permission from [62]. Copyright ©SPIE 2005.

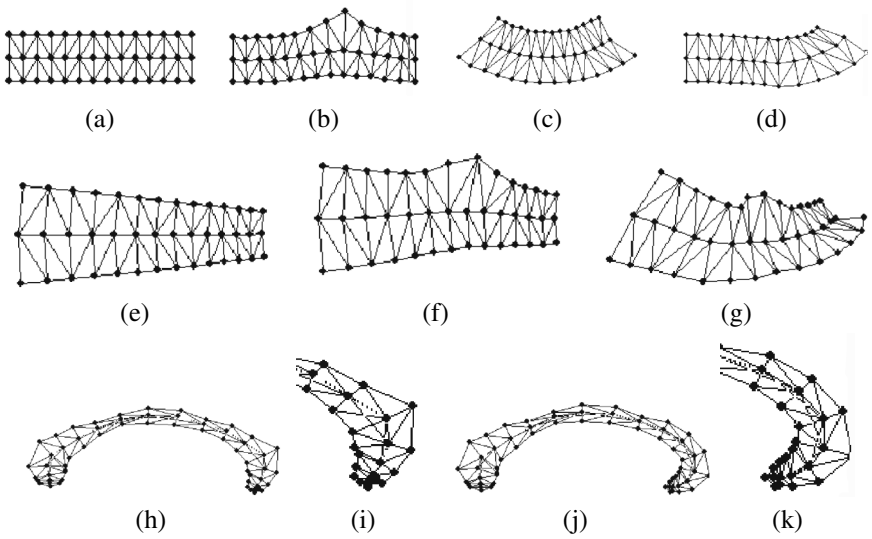

Figure 25. Examples of localized deformations: (a) initial synthetic object, (b) bulge, (c) bend, (d) bend at another location, (e) tapering, (f) tapering followed by a bulge, and (g) tapering followed by a bulge and a bend deformations. CC model (h) before and (j) after a localized bend. (i,k) Close-up versions of (h,j). Reprinted with permission from [62]. Copyright ©2003, SPIE.

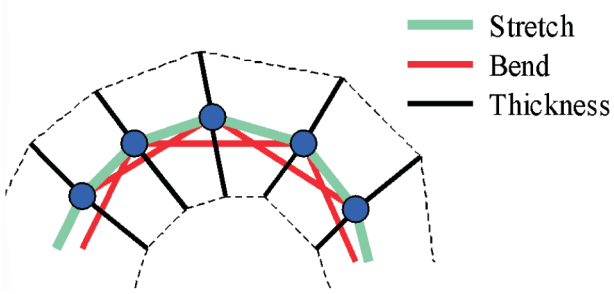

Figure 26. Spring types used for statistics-based deformations. Reprinted with permission from [62]. Copyright ©2003, SPIE.

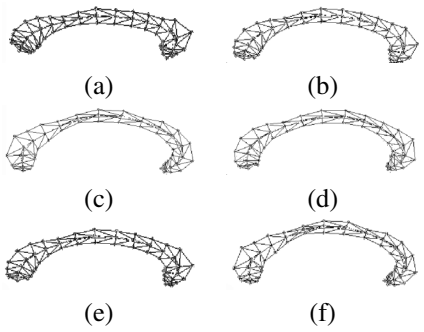

Figure 27. Sample corpus callosum mesh model deformations (1st PC for all deformation types over the entire CC) derived from the hierarchical regional PCA. Reprinted with permission from [62]. Copyright ©2003, SPIE.

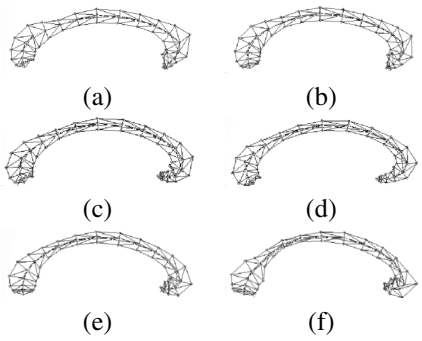

Figure 28. Sample CC mesh model deformations (2nd PC for all deformation types over the entire CC) derived from the hierarchical regional PCA. Reprinted with permission from [62]. Copyright ©2003, SPIE.

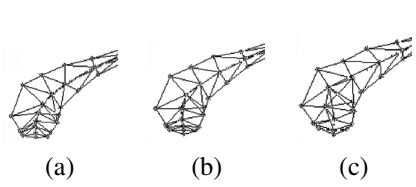

Figure 29. Statistical CC mesh model deformations: stretching the splenium. Reprinted with permission from [62]. Copyright ©2003, SPIE.

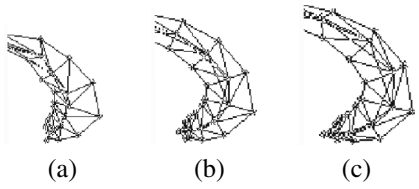

Figure 30. Statistical CC mesh model deformations: bending the genu. Reprinted with permission from [62]. Copyright ©2003, SPIE.

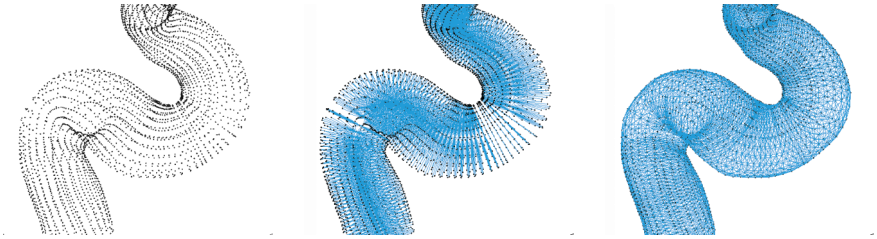

Figure 31. Topology of the vessel crawler showing: Masses (left), radial springs (middle), and stability springs (right) across sequential layers of the organism.

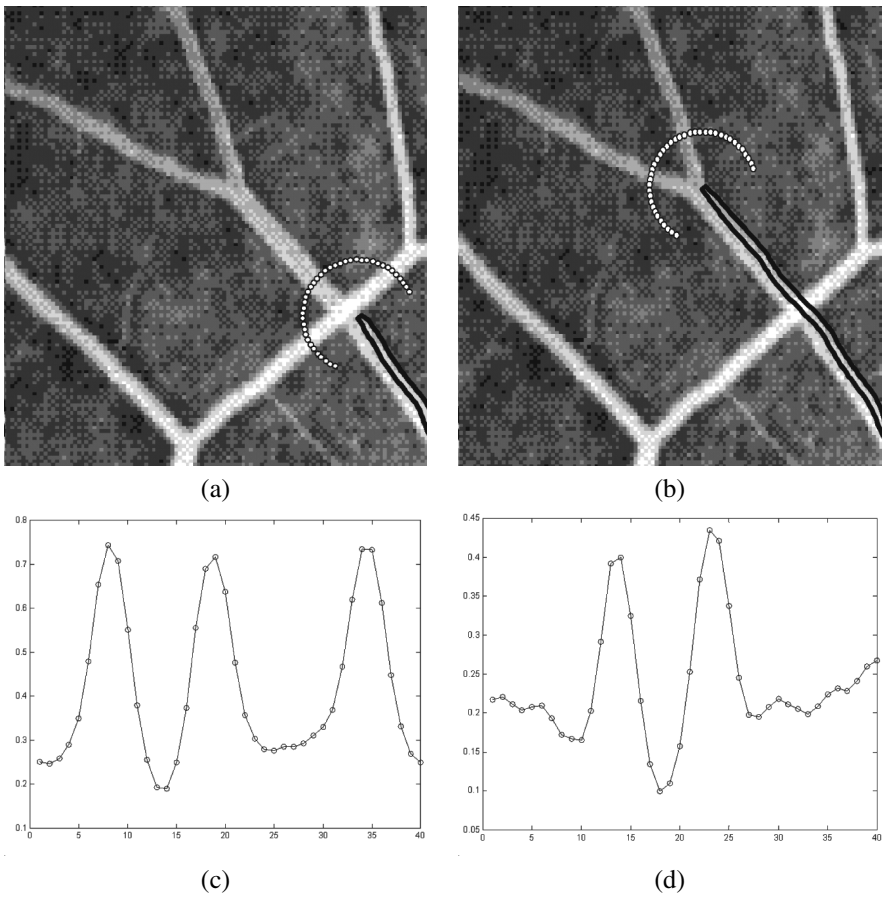

Figure 32. Off-board sensors (arc of white nodes in (a) and (b)) measure image intensity (along the arc). This results in an intensity profile exhibiting three distinct peaks when an overlapping vessel is ahead (c) and only two peaks in the case of a bifurcation (d).

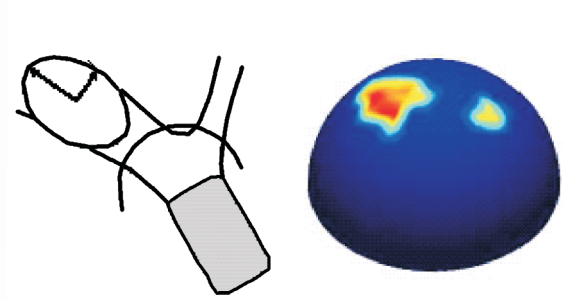

Figure 33. A vessel crawler (left, in gray) utilizing an off-board hemispherical sensor (shown as an arc in the left-hand image). The sensor (shown in 3D on the right) collects vesselness measures, guiding it as it crawls along the vessel and detects branching points.

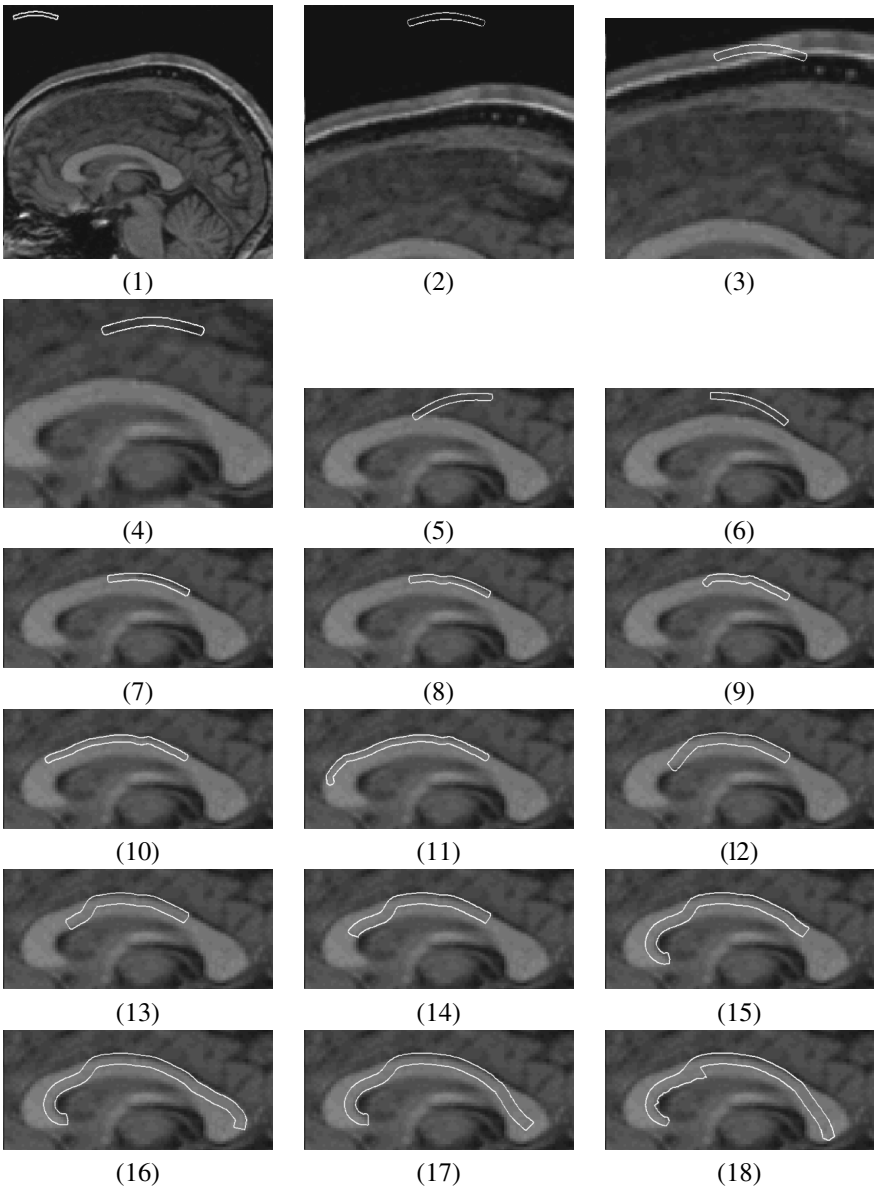

Figure 34. Deformable corpus callosum organism progressing through a sequence of behaviors to segment the CC (results continued on next page). Reprinted with permission from [85]. Copyright ©2002, Elsevier.

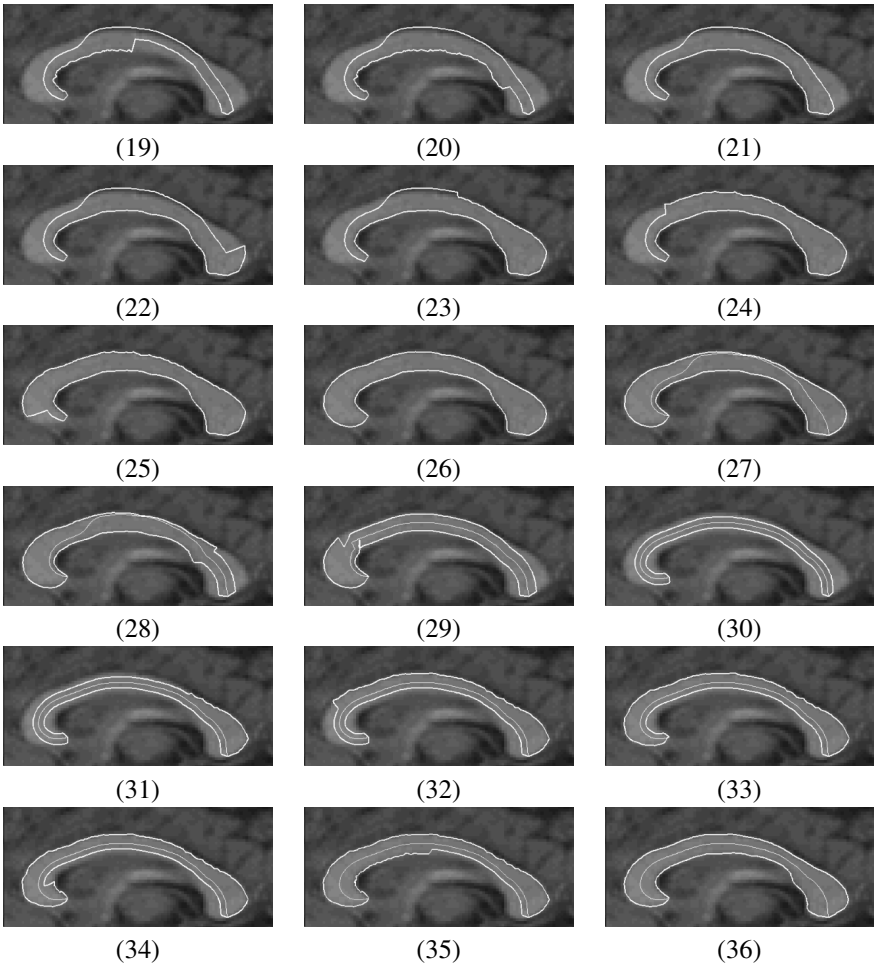

Figure 34. (continued). Results continued from previous page.

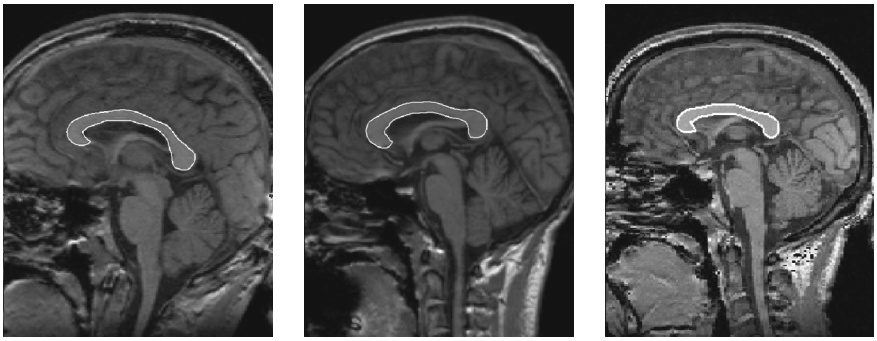

Figure 35. Segmentation results. Reprinted with permission from [38]. Copyright ©2002, Springer.

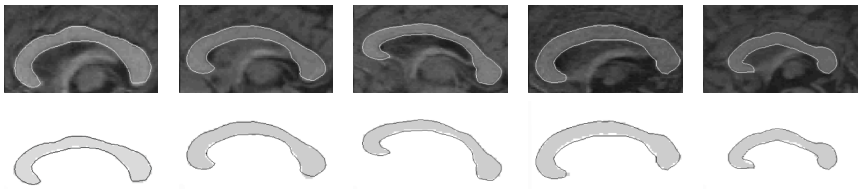

Figure 36. Segmentation results (top), also shown (in black) over manually segmented (gray) corpora callosa (bottom). Reprinted with permission from [85]. Copyright ©2002, Elsevier.

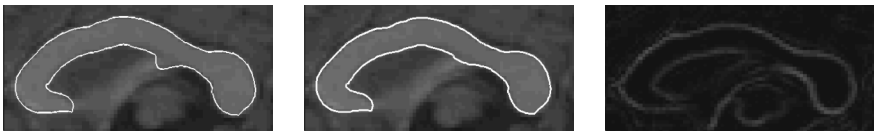

(a) (b) (c)

Figure 37. Segmentation result (a) before and (b) after detecting and repairing the fornix dip. (c) Note the weak gradient magnitude where the fornix overlaps the CC. Reprinted with permission from [85]. Copyright ©2002, Elsevier.

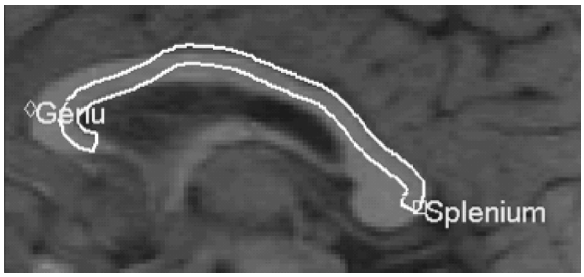

Figure 38. The CC organism's self-awareness enables it to identify landmark parts. Reprinted with permission from [85]. Copyright ©2002, Elsevier.

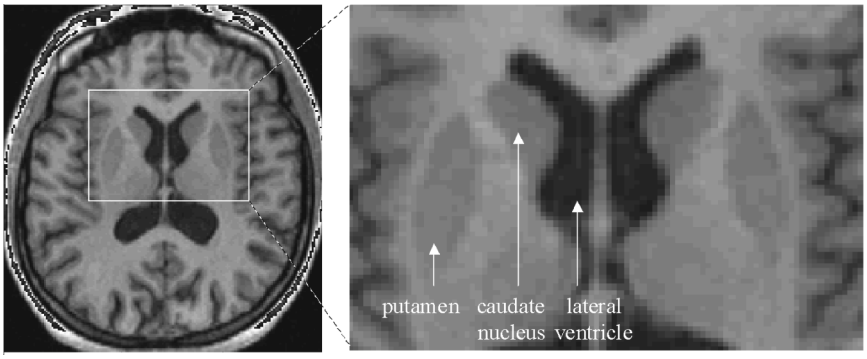

Figure 39. The lateral ventricle, caudate nucleus, and putamen shown in transversal brain MRI slice.

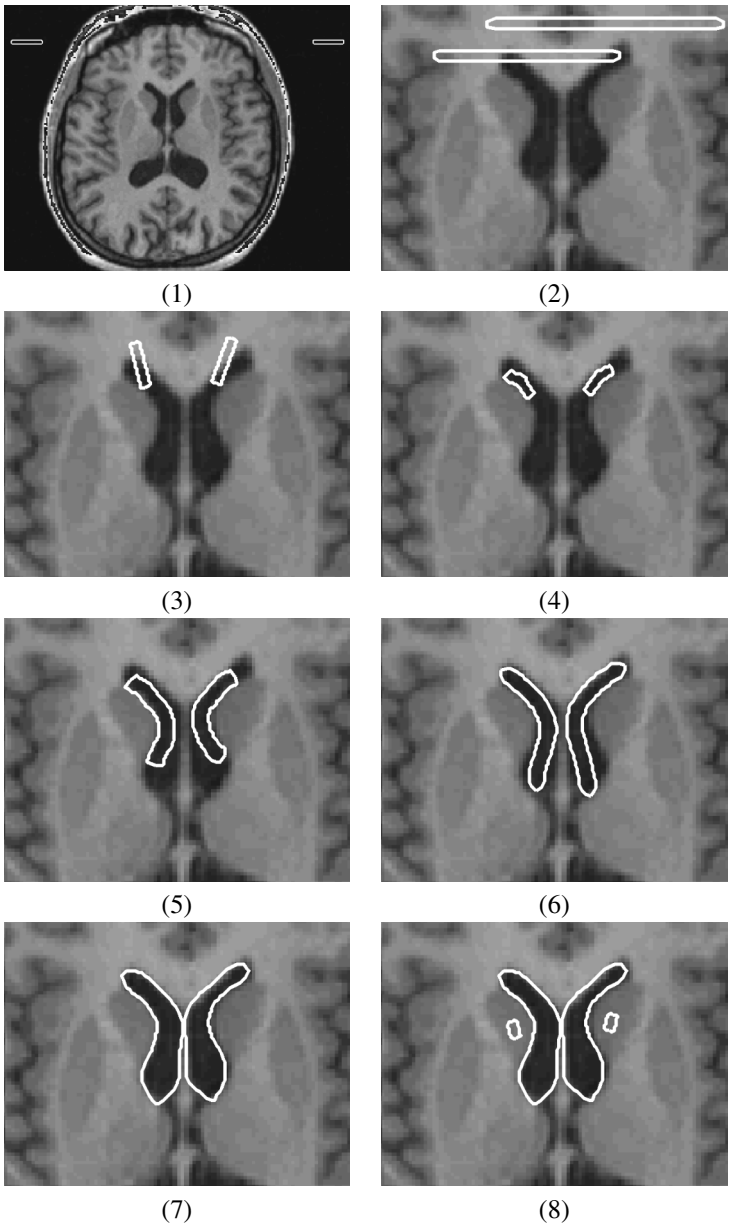

Figure 40. Deformable lateral ventricles (1–16), caudate nuclei (CN) (8–16), and putamina (11-16) organisms progressing through a sequence of behaviors to locate the corresponding structures in an MR brain image. Reprinted with permission from [85]. Copyright ©2002, Elsevier. (results continued on next page)

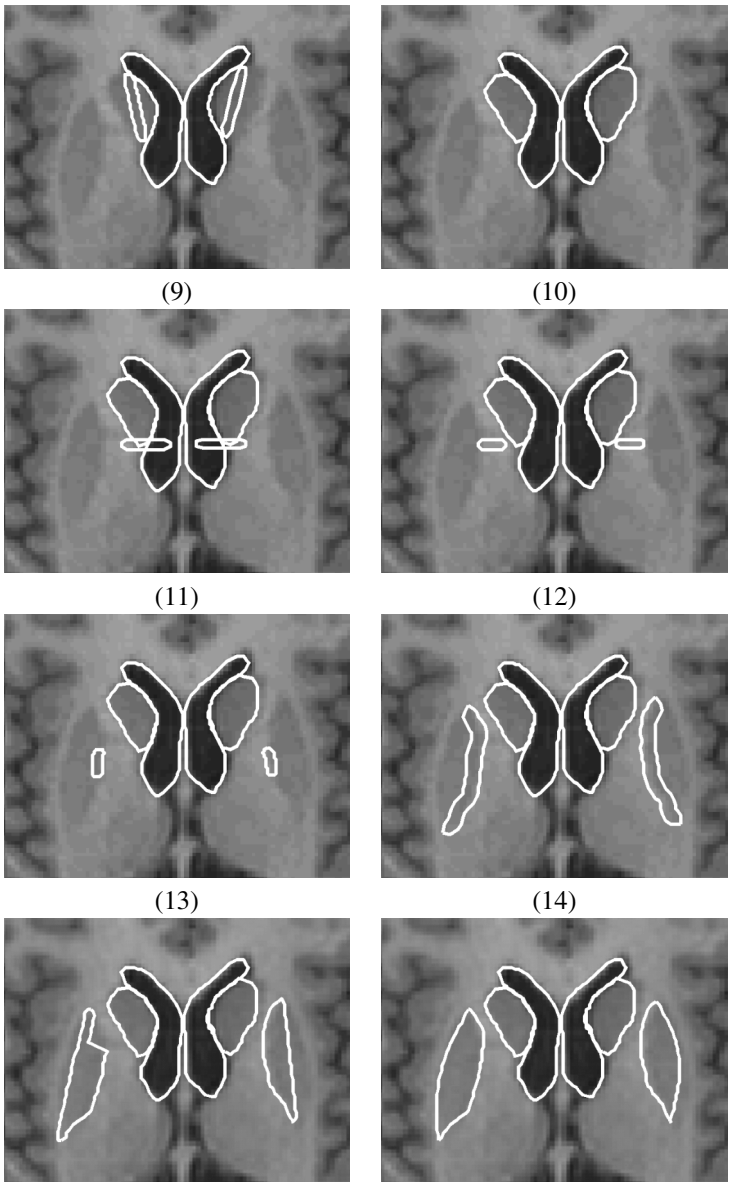

Figure 40. (continued). Results continued from previous page.

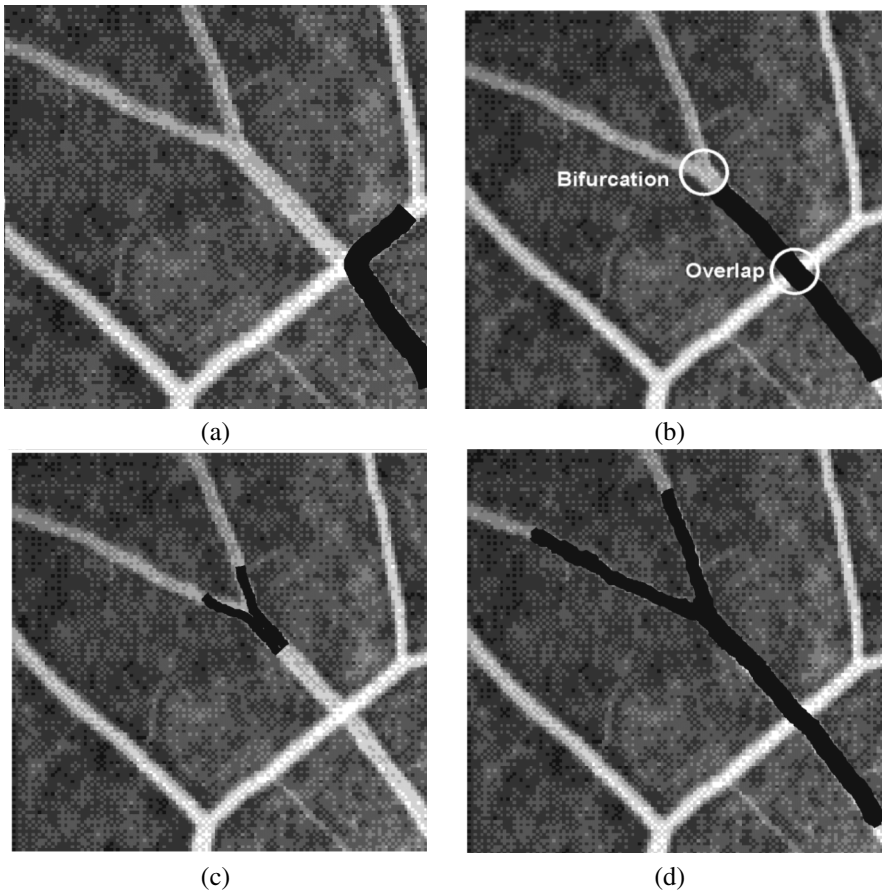

Figure 41. Segmenting vessels in an angiogram. (a) A deformable organism turning right and latching onto the wrong overlapping vessel. (b) High-level constraints enable the organism to differentiate between overlapping vessels and bifurcations. (c) Two new organisms are born upon identifying a bifurcation. (d) The segmented main vessel and its two branches. Reprinted with permission from [85]. Copyright ©2002, Elsevier.

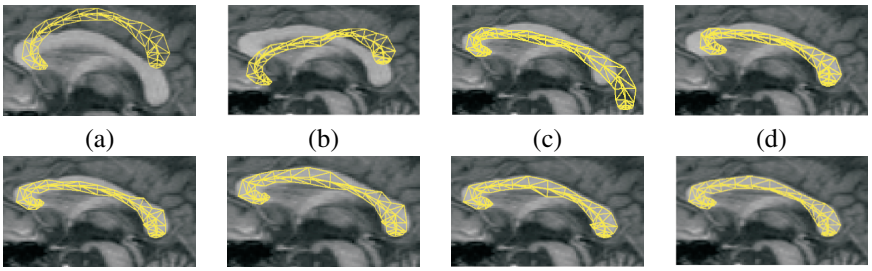

Figure 42. Progress of segmentation through its primary phases: (a) global model alignment, (b) model part alignment through (c) expansion and (d) contraction, (e) medial-axis alignment, (f) fitting to boundary, (g) detecting and (h) repairing fornix dip. Reprinted with permission from [80]. Copyright ©2005, SPIE.

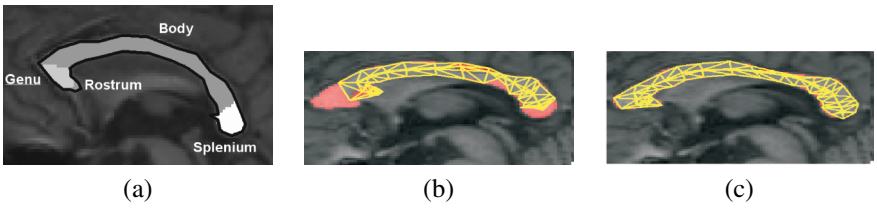

Figure 43. (a) Automatic labeling of important anatomical regions of the CC. (b) Before and (c) after intuitive manual intervention to improve the segmentation (red color corresponds to areas of erroneous segmentation). Reprinted with permission from [80]. Copyright ©2005, SPIE.

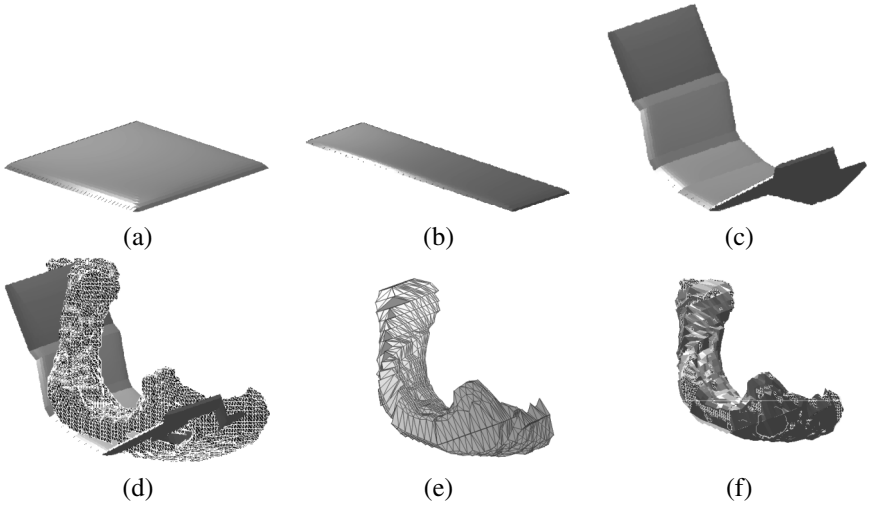

Figure 44. Fitting a 3D shape model to a lateral ventricle: (a) initial 3D model, (b) uniform shrinking along the x-axis, (c) bending deformations, (d) medial sheet bent into approximate bisecting position of target structure, (e) final 3D shape reconstructed from the medial sheets, and (f) overlay of 3D model on target structure.

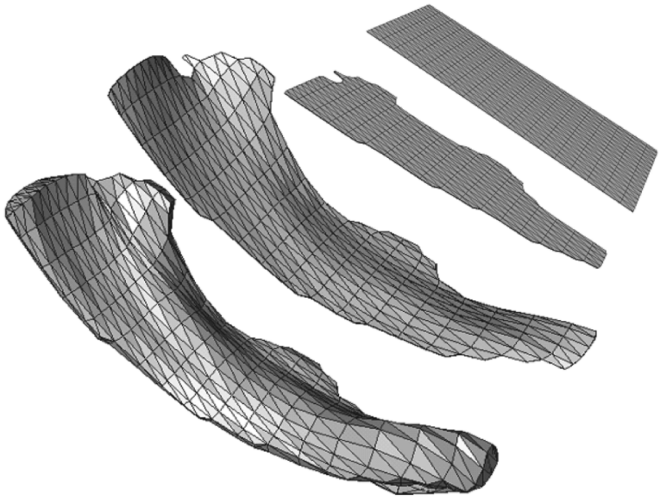

Figure 45. Caudate nucleus (CN) represented using a medial patch. Top to bottom: initial rectangular planar medial sheet, planar sheet cropped to match CN projection, curved medial sheet placed equidistant from the upper and lower CN boundaries. Thickness values are associated with each node in the medial sheet yielding a 3D surface of the CN.

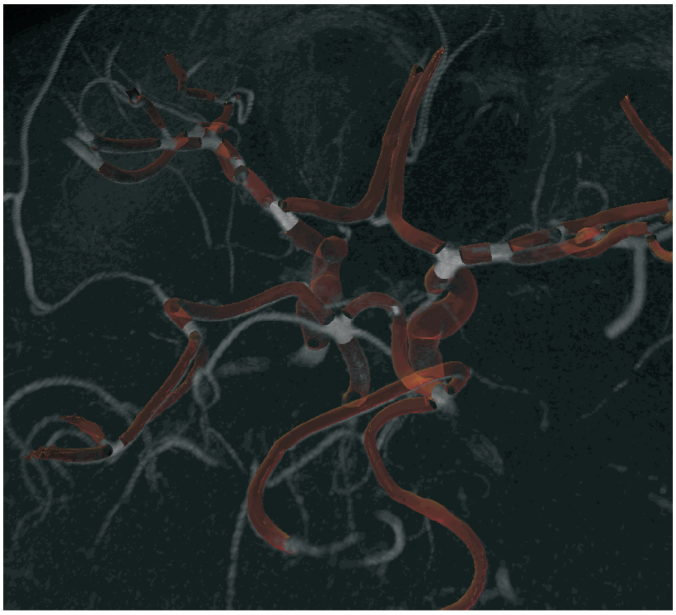

Figure 46. Maximum intensity projection rendering of an MRA showing the vessel crawler in orange.

Figure 47. Three example representations of a vascular system: directed acyclic graph (left), a plot of the vessels with color corresponding to radial thickness (top), and a tree representing to the structure of a segmented vessel (bottom).